Pharmaceutical Research, Vol. 24, No. 6, June 2007 (© 2007)
DOI: 10.1007/s11095-006-9220-1

Research Paper

In Vivo Performance of a Liposomal Vascular Contrast Agent for CT and MR-Based Image Guidance Applications

Jinzi Zheng,[1] Jubo Liu,[2] Mike Dunne,[2] David A. Jaffray,[1,3,4] and Christine Allen[2,5,6,7]

Received September 28, 2006; accepted December 15, 2006; published online March 21, 2007

Purpose. This study evaluated the *in vivo* performance of a liposome formulation that co-encapsulates iohexol and gadoteridol as a multimodal contrast agent for computed tomography (CT) and magnetic resonance (MR)-based image guidance applications.
Materials and Methods. The pharmacokinetics and biodistribution studies were conducted in Balb-C mice using high performance liquid chromatography (HPLC) and inductively coupled plasma atomic emission spectrometry (ICP-AES) to detect iohexol and gadoteridol concentrations. The imaging efficacy of this liposome system was assessed in New Zealand White rabbits using a clinical CT and a clinical 1.5 Tesla MR scanner.
Results. The vascular half-lives of the liposome encapsulated iohexol and gadoteridol in mice were found to be 18.4±2.4 and 18.1±5.1 h. When administered at the same dose the distribution (α phase) half-lives for the free contrast agents were 12.3±0.5 min (iohexol) and 7.6±0.9 min (gadoteridol); while, the elimination (β phase) half-lives were 3.0±0.9 h for free iohexol and 3.0±1.3 h for free gadoteridol. The CT and MR signal increases were measured and correlated with the concentrations of iohexol and gadoteridol detected in plasma samples.
Conclusion. The long *in vivo* circulation lifetime and simultaneous CT and MR signal enhancement provided by this liposome system make it a promising agent for image guidance applications.

KEY WORDS: computed tomography; contrast agent; liposome; magnetic resonance imaging; multimodality imaging.

INTRODUCTION

There has been a tremendous growth in the use of non-invasive imaging techniques for characterization of biological processes, diagnosis of disease and guidance of interventions or treatment. Examples of image guided interventions include X-ray, MR and ultrasound-guided surgical procedures (1–4), as well as cone-beam CT-based guidance of radiation therapy delivery (5,6). Although different imaging techniques are able to detect inherent contrast in biological systems, conventional diagnostic agents have been employed to enhance soft tissue contrast (7,8). However, these are typically low molecular weight molecules and their rapid clearance creates the need for multiple administrations (i.e., angiography). The development of a long circulating contrast agent would offer benefits for guiding interventions in which multiple injections are not feasible or the imaging procedure requires more persistent signal enhancement. Specifically, in radiation therapy, volumetric CT and MR data sets are first acquired and registered for the purpose of radiation dose calculation and target definition (9), and cone-beam CT is then used to guide the delivery of radiation at each treatment session (5,6). In this application, the contrast agent is required to provide prolonged signal enhancement for planning (CT and MR), as well as visibility during the process of cone-beam CT acquisition. Thus, an agent with an *in vivo* lifetime of several days or even weeks would be ideal.

A viable strategy to achieve prolonged signal enhancement *in vivo* is to employ colloidal vehicles to carry conventional contrast agents. Indeed, nano-sized contrast agents have been engineered using liposomes (10–19), lipid and polymeric micelles (20–24), nanoparticles (25–30), dendrimers (31–34) and proteins (35,36) as carrier systems. In a few cases, these systems have been designed to provide simultaneous contrast enhancement in multiple modalities (14,18,37–39). However, none of the colloidal systems reported to date have been demonstrated to provide satisfactory and simultaneous signal enhancement in CT and MR.

[1] Department of Medical Biophysics, University of Toronto, Toronto, Ontario, Canada.
[2] Department of Pharmaceutical Sciences, University of Toronto, 144 College Street, Room 1203, Toronto, Ontario M5S 3M2, Canada.
[3] Radiation Medicine Program, Ontario Cancer Institute/Princess Margaret Hospital, University Health Network, Toronto, Ontario, Canada.
[4] Department of Radiation Oncology, University of Toronto, Toronto, Ontario, Canada.
[5] Department of Chemistry, University of Toronto, Toronto, Ontario, Canada.
[6] Department of Chemical Engineering and Applied Chemistry, University of Toronto, Toronto, Ontario, Canada.
[7] To whom correspondence should be addressed. (e-mail: cj.allen@utoronto.ca)

Also, the limited *in vivo* stability and circulation lifetime of these systems prevent their use throughout both the planning and delivery of radiation therapy.

In a previous report, our group summarized the development and *in vitro* characterization of a dual modality contrast agent for imaging in CT and MR (18). The agent consists of liposomes co-encapsulating iohexol, an iodine-based conventional CT agent, and gadoteridol, a gadolinium-based conventional MR agent within their internal aqueous compartment. The liposome-based system exhibited high stability *in vitro*, with less than 10% of the total amount of the encapsulated agents (i.e., iohexol and gadoteridol) released over a 14-day period in physiological buffer at 37°C. The present study is aimed at investigating the *in vivo* pharmacokinetics and imaging characteristics of this dual modality agent. Specifically, the *in vivo* stability was evaluated by measuring the pharmacokinetics and biodistribution of the liposome encapsulated CT and MR agents in Balb-C mice following intravenous (i.v.) administration. Studies evaluating the *in vivo* imaging efficacy were conducted in New Zealand White rabbits using clinical CT and MR scanners. In addition, the signal increases measured in a region of interest in the rabbit aorta in the two imaging modalities were correlated with the actual iodine and gadolinium concentrations detected in plasma samples in order to investigate the potential of using this agent for quantitative imaging applications.

MATERIALS AND METHODS

Materials

1,2-Dipalmitoyl-*sn*-Glycero-3-Phosphocholine (DPPC, M.W. 734), and 1,2-Distearoyl-sn-Glycero-3-Phosphoethanolamine-N-[Poly(ethylene glycol)2000] (PEG_{2000}DSPE, M.W. 2774) were purchased from Genzyme Pharmaceuticals (Cambridge, MA, USA). Cholesterol (CH, M.W. 387) was purchased from Northern Lipids Inc. (Vancouver, British Columbia, Canada). The CT contrast agent Omnipaque® (Nycomed Imaging AS, Oslo, Norway) has an iodine concentration of 300 mg/mL and consists of the non-ionic, iodinated molecule iohexol (N, N′-Bis(2,3-dihydroxypropyl)-5-[N-(2,3-dihydroxypropyl)-acetamido]-2,4,6-triiodo-isophthalamide, M.W. 821.14, 3 iodine atoms per molecule) dissolved in an aqueous solution with tromethamine and edentate calcium disodium. The MR contrast agent ProHance® (Bracco Diagnostics Inc., Princeton, NJ, USA) has a gadolinium concentration of 78.6 mg/mL and consists of the non-ionic, gadolinium complex gadoteridol (10-(2-hydroxy-propyl)-1,4,7,10-tetraazacyclododecane-1,4,7-triacetic acid, M.W. 558.7, 1 gadolinium atom per complex) dissolved in an aqueous solution with calteridol calcium and tromethamine.

Preparation and Characterization of Liposome Formulations

Liposomes composed of DPPC, cholesterol and PEG_{2000} DSPE in 55:40:5 %mol ratios were prepared according to a method described in detail elsewhere (18). Briefly, 100 mmol/L of the lipid mixture was first dissolved in an initial ethanol volume corresponding to 10% of the desired final sample volume. Omnipaque® and Prohance® were then added to the lipid mixture at a volume ratio of 4:1 and left to hydrate at 75°C for at least 4 h. The resulting multilamellar vesicles were then sized to 70–85 nm in diameter using high pressure extrusion (ten extrusion cycles) at 70°C with a 10 mL Lipex™ Extruder (Northern Lipids Inc., Vancouver, British Columbia, Canada). The un-encapsulated iohexol and gadoteridol molecules were removed by membrane dialysis (8,000 molecular weight cut-off) for 8 h against 250-fold excess volume of N-(2-hydroxyethyl)piperazine-N'(ethanesulfonic acid) (HEPES) buffer saline (HBS). The size of the liposomes was measured by dynamic light scattering (DLS) analysis of dilute solutions using a DynaPro DLS instrument (Protein Solutions, Charlottesville, VA, USA) at 25°C. The final concentration of iohexol was determined using a UV assay with detection at a wavelength of 245 nm (Helios γ, Spectronic Unicam, MA, USA). The final concentration of gadoteridol was determined using an assay based on inductively coupled plasma atomic emission spectrometry (ICP-AES Optima 3000DV, Perkin Elmer, MA, USA) (18).

Pharmacokinetics and Biodistribution Studies

The pharmacokinetics and biodistribution studies were performed under protocols approved by the University Health Network Animal Care and Use Committee. Female Balb-C mice (8–12 weeks, 18–23 g) were administered slow bolus tail vein injections of 150 μL of contrast agent. Each mouse received 650 mg/kg of iohexol (equivalent to 300 mg/kg iodine) and 60 mg/kg gadoteridol (equivalent to 17 mg/kg of gadolinium) either as a mixture of free agents diluted in HBS or co-encapsulated in liposomes. The animals were anaesthetized with 2% isoflurane and a terminal blood volume (0.5–1.0 mL) was drawn by cardiac puncture at 5, 15, 30 min and 1, 2 and 3 h following the administration of the free agent mixture, and at 5 min, 1, 8, 24, 48, 72, 96, 120, 144 and 168 h following administration of the liposome formulation. The animals were then sacrificed by cervical dislocation and their heart, liver, kidneys and spleen were harvested. Each organ was thoroughly washed in phosphate buffer saline (PBS, pH=7.4) and then frozen at −80°C.

The plasma was isolated by centrifugation of the blood samples at 3,000 g for 10 min. Iohexol and gadoteridol were extracted from the plasma and tissue samples using 10% perchloric acid (4-fold excess volume). Plasma and tissue concentrations of iohexol were determined using a high performance liquid chromatography instrument (HPLC, PerkinElmer Series 200) equipped with a C18 Xterra reverse-phase column with ρ-aminobenzoic acid as the internal standard. The mobile phase for plasma samples was 90% methanol and 10% 100 mM acetic acid buffer at a pH of 4.10. The mobile phase for tissue samples was composed of 92% methanol and 8% 100 mM acetic acid buffer at a pH of 4.10. The flow rate was 0.9 mL/min and UV detection was performed at 245 nm to measure the concentration of iohexol. The plasma and tissue concentrations of gadoteridol were determined using ICP-AES (18).

The data obtained from the pharmacokinetics study was used to determine the main pharmacokinetic parameters for iohexol and gadoteridol when administered as free agents or

agents encapsulated within liposomes. For the free agents, a two-compartment model was used to determine the distribution constant (K_d or α) and the elimination constant (K_e or β). The distribution half-life $(t_{1/2\alpha})$ was then calculated using the equation: $(t_{1/2\alpha}) = \ln(2)/K_d$, while the elimination half-life $(t_{1/2\beta})$ was calculated using the equation: $(t_{1/2\beta}) = \ln(2)/K_e$. For the liposome encapsulated agents, the K_e value was determined by fitting the plasma concentration versus time curve (each data point represents the mean of three distinct animals) with a one-compartment model. The vascular circulation half-life ($t_{1/2}$) was then calculated using the following equation: $t_{1/2} = \ln(2)/K_e$. The area under the plasma concentration versus time curve (AUC) was calculated using the trapezoid rule. The plasma clearance CL and the volume of distribution V_d were determined using Eqs. 1 and 2, respectively, as shown below.

$$CL = \frac{Dose}{AUC \cdot BodyWeight} \tag{1}$$

$$V_d = \frac{CL}{K_e} \tag{2}$$

Due to the inadequate resolution of the clinical CT and 1.5 T MR (and head coil) systems for imaging mouse vasculature, a larger animal model (rabbit) was employed for the following imaging studies.

CT and MR Imaging of Animal Subjects

The *in vivo* imaging study was performed under a protocol approved by the University Health Network Animal Care and Use Committee. Healthy female New Zealand White rabbits (2.5–3 kg) were anaesthetized with an intramuscular injection of either a ketamine and xylazine mixture or acepromazine. A slow bolus injection (0.5 mL/second) of 20 mL of the liposomal contrast agent formulation was then administered to the marginal ear vein catheter. Each rabbit received 730 mg/kg iohexol (equivalent to 340 mg/kg of iodine) and 69 mg/kg gadoteridol (equivalent to 19 mg/kg of gadolinium) co-encapsulated within the liposomes. 2% isoflurane vapor was given by inhalation throughout the study. Images of the rabbits were acquired pre and post-administration of the liposome formulation in CT (GE Discovery ST, General Electric Medical Systems, Milwaukee, WI, USA) and MR (GE Signa TwinSpeed MR scanner, General Electric Medical Systems, Milwaukee, WI, USA). The rabbits were CT scanned (120 kVp, 200 mA, a voxel size of $0.43\times0.43\times0.625$ mm^3, and a FOV of $220\times220\times400$ mm^3) at 10 and 60 min as well as 24, 48, 72, 96, 120 and 168 h following administration of the liposome formulation. The rabbits were MR scanned (3D FSPGR sequence with a TR of 9.8 ms, a TE of 4.3 ms, a flip angle of 15°, a voxel size of $0.86\times0.86\times1.5$ mm^3 over a FOV of $220\times220\times228$ mm^3, and an image matrix of 256×256) at 30 and 90 min as well as 24, 48, 72, 96, 120 and 168 h post-administration of the formulation. The mean attenuation values in Hounsfield units (HU) in CT and the relative signal intensities (SI) in MR were measured in the aorta with circular regions of interest of over a cross sectional area of ~9 mm^2 in a single axial image. For visualization purposes, 3D maximum intensity projection (MIP) images were generated using eFilm Workstation (Merge eFilm, Milwaukee, WI, USA). The same window and level were used for the pre and post-contrast images. In addition, for the correlation study, 1.5 mL of blood was collected from the ear vein of the same rabbits at the following time points: 5 min, 24, 48, 72, 96, 120 and 168 h.

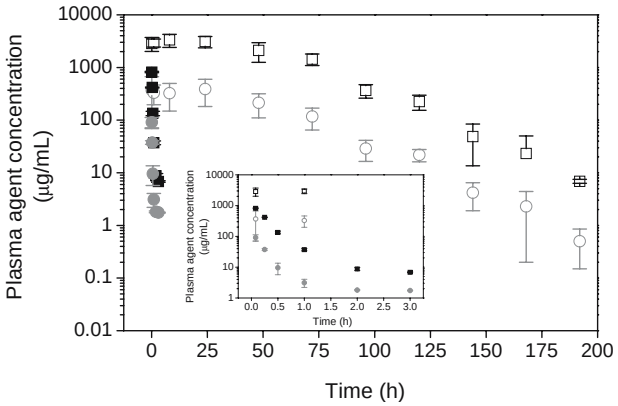

Fig. 1. Pharmacokinetics of free iohexol (■), free gadoteridol (●), liposomal iohexol (□) and liposomal gadoteridol (○) in healthy female Balb-C mice (n=3). The 2-week-old mice (18–23 g) were i.v. administered free iohexol and free gadoteridol diluted in HBS or liposome encapsulated iohexol and gadoteridol containing 650 mg/kg of iohexol (equivalent to 300 mg/kg iodine) and 60 mg/kg gadoteridol (equivalent to 17 mg/kg of gadolinium). Plasma was sampled at the indicated time points and analyzed using HPLC for iohexol and ICP-AES for gadoteridol. Data are represented as the mean±standard deviation.

Table I. Pharmacokinetic Parameters for Iohexol and Gadoteridol When Administered in a Liposome Formulation to Female Balb-C Mice

	Iohexol	Gadoteridol
K_e	0.0377	0.0383
r^2	0.975	0.980
$t_{1/2}$ (h)	18.4	18.1
AUC (μg*h/mL)	5910000	582000
CL (mL/h/g)	0.00219	0.00206
V_d (mL/g)	0.0580	0.0538

Abbreviations: K_e is the elimination constant; r^2 is the coefficient of determination for this fit (every point used for the fit is the mean value obtained from three distinct animals); $t_{1/2}$ is the vascular circulation half-life; AUC is the area under the concentration versus time curve in plasma; CL is the total plasma clearance and V_d is the volume of distribution per unit mass.

Acute Toxicity Studies and Corresponding Statistical Analysis

Female Balb-C mice (8–12 weeks, 18–20 g) were randomly divided into three groups as follows: mice receiving no formulation, mice receiving empty liposomes (530 mg/kg of lipid); mice receiving iohexol (650 mg/kg, equivalent to 300 mg/kg iodine) and gadoteridol (53 mg/kg, equivalent to 15 mg/kg gadolinium) co-encapsulated within liposomes (530 mg/kg

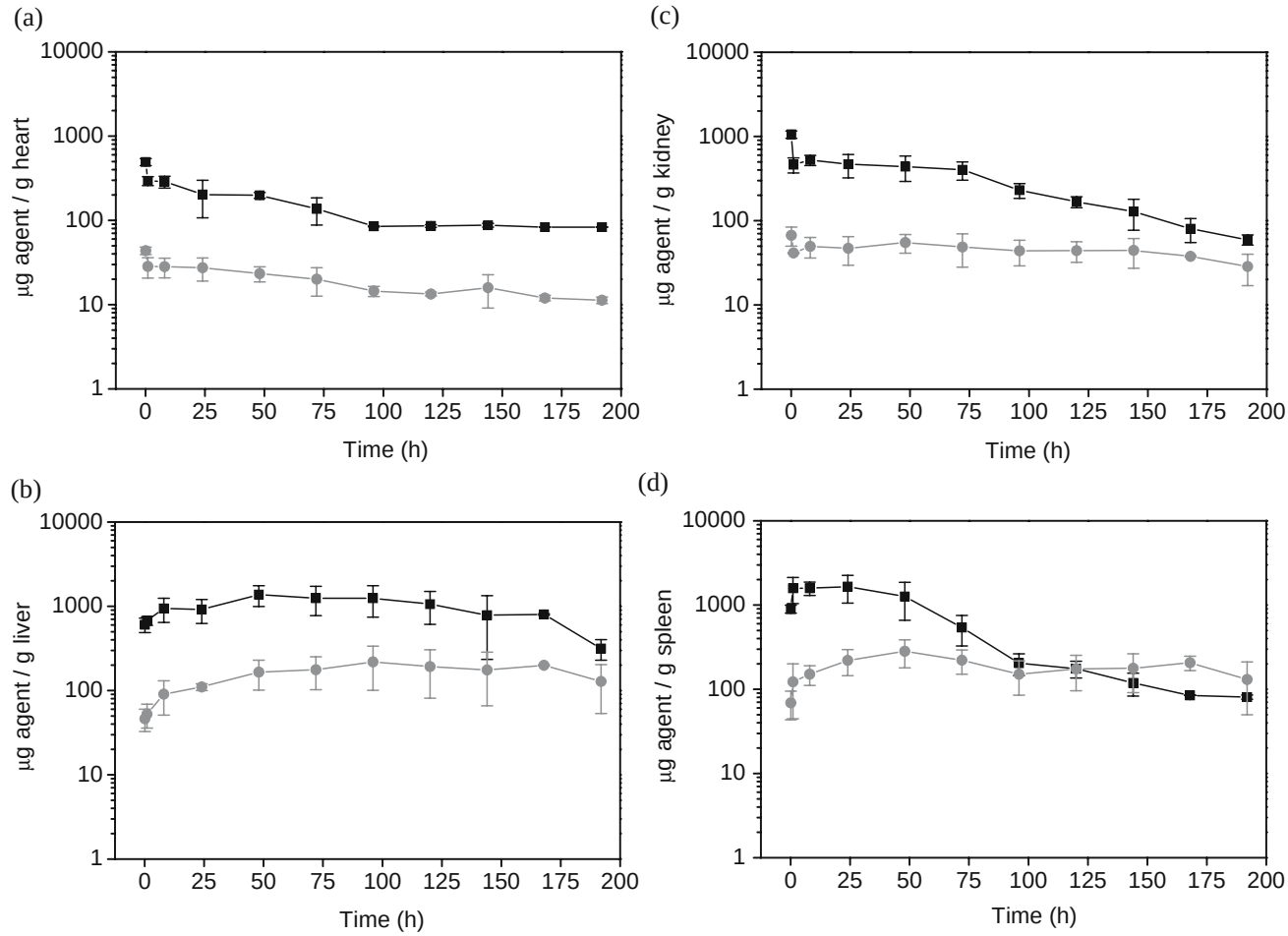

Fig. 2. Biodistribution of iohexol (■) and gadoteridol (●) when administered in a liposome formulation to female Balb-C mice. The animals were sacrificed at specific times and **a** heart, **b** liver, **c** kidneys, **d** spleen samples were analyzed to determine levels of iohexol and gadoteridol. Each data point represents the mean of three distinct animals±standard deviation.

lipid). Seven days later blood samples (0.5–1 mL) were drawn by cardiac puncture and sent to Vita-Tech (Markham, Ontario, Canada) for haematological and biochemical analysis. The analysis included determination of number of white and red blood cells (WBC and RBC), platelets, and measurement of hematocrit, hemoglobin, serum creatinine, alkaline phosphatase (ALP), alanine transaminase (ALT) and aspartate transaminase (AST) concentrations. Statistical comparisons of the acute toxicity values were performed using the student *t*-test (40). Computations were performed in Microsoft Excel.

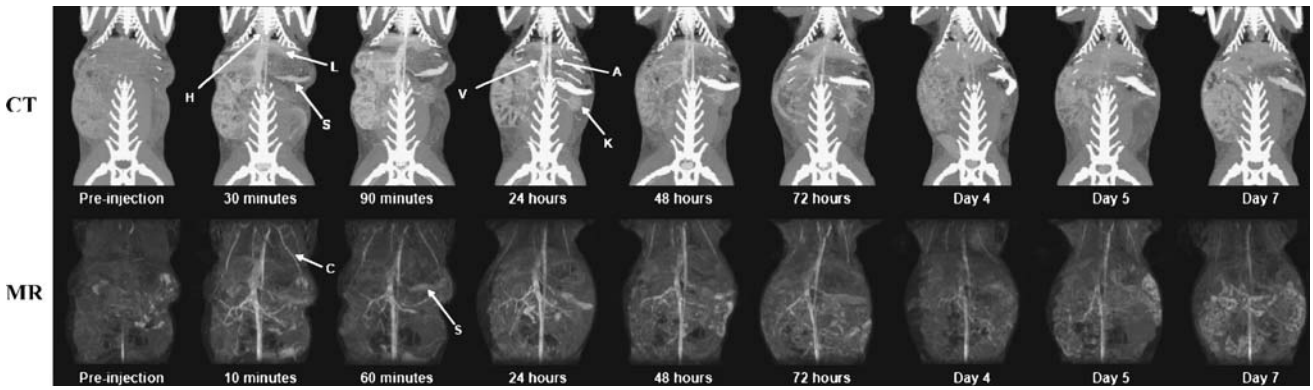

Fig. 3. Three-dimensional maximum intensity projection images (*anterior view*) of a healthy New Zealand White rabbit (3 kg) obtained in CT (120 kV, 200 mA) and MR (3D FSPGR sequence, TR/TE=9.8/4.3) prior to and following i.v. administration (as indicated) of the liposome formulation of iohexol and gadoteridol. The same window and level were used for pre- and post-injection images. Note the visual contrast changes in the heart (H), aorta (A), vena cava (V), carotid artery (C), kidney (K) and spleen (S).

P-values greater than 0.05 were considered to be statistically insignificant.

RESULTS

Preparation and Characterization of the Multimodal Liposome Formulation

The preparation, physico-chemical characterization and *in vitro* optimization of this multimodal liposome formulation have been described in detail elsewhere (18). The average diameter of the liposomes in each preparation, as measured by DLS, was found to range between 70–85 nm. Each formulation contained an iodine to lipid weight ratio of 1:1.8 and gadolinium to lipid weight ratio of 1:35. The iodine to gadolinium ratio employed in this formulation was selected from consideration of *in vitro* imaging studies in phantoms, which evaluated the sensitivity of each imaging modality to detect the presence of contrast material within the formulation (18).

Pharmacokinetics and Biodistribution Studies in Healthy Mice

The pharmacokinetics and organ distribution profiles of the co-encapsulated contrast agents, iohexol and gadoteridol, were evaluated in healthy female Balb-C mice as a means to assess the *in vivo* stability of this liposome formulation. Figure 1 includes the 7-day pharmacokinetics profiles for iohexol and gadoteridol, following i.v. administration in the DPPC/CHOL/PEG_{2000}DSPE liposomes, as well as the 3-h pharmacokinetics profiles for free iohexol and gadoteridol. The pharmacokinetics profiles for the agents encapsulated in liposomes were fit using a one-compartment model and the main pharmacokinetics parameters were calculated as listed in Table I. The circulation half-lives for the agents were found to be 18.4±2.4 h for liposome encapsulated iohexol and 18.1±5.1 h for liposome encapsulated gadoteridol. The pharmacokinetics profiles for the free agents were fit using a two-compartment model. The distribution (α phase) half-life for free iohexol was 12.3±0.5 min and for free gadoteridol it was 7.6±0.9 min, while the elimination (β phase) half-lives were 3.0±0.9 h for free iohexol and 3.0±1.3 h for free gadoteridol. The values obtained for the half-lives of the free agents are in agreement with previously published results (41,42). The extended and similar circulation half-lives obtained for iohexol and gadoteridol when administered in this liposome formulation suggest that these agents remain co-encapsulated within the formulation *in vivo*.

Figure 2 includes biodistribution profiles for the liposome-encapsulated agents in the heart, liver, kidney and spleen over a 7-day period. Similar distribution and clearance behavior were seen in the heart and liver for iohexol and gadoteridol. While an enhanced elimination of iohexol was observed in the kidney and the spleen compared to gadoteridol.

In Vivo CT and MR Imaging in Healthy Rabbits

Imaging studies were performed on rabbits with a clinical CT scanner and a clinical MR scanner with a head coil. As shown in Fig. 3, the same rabbit was imaged

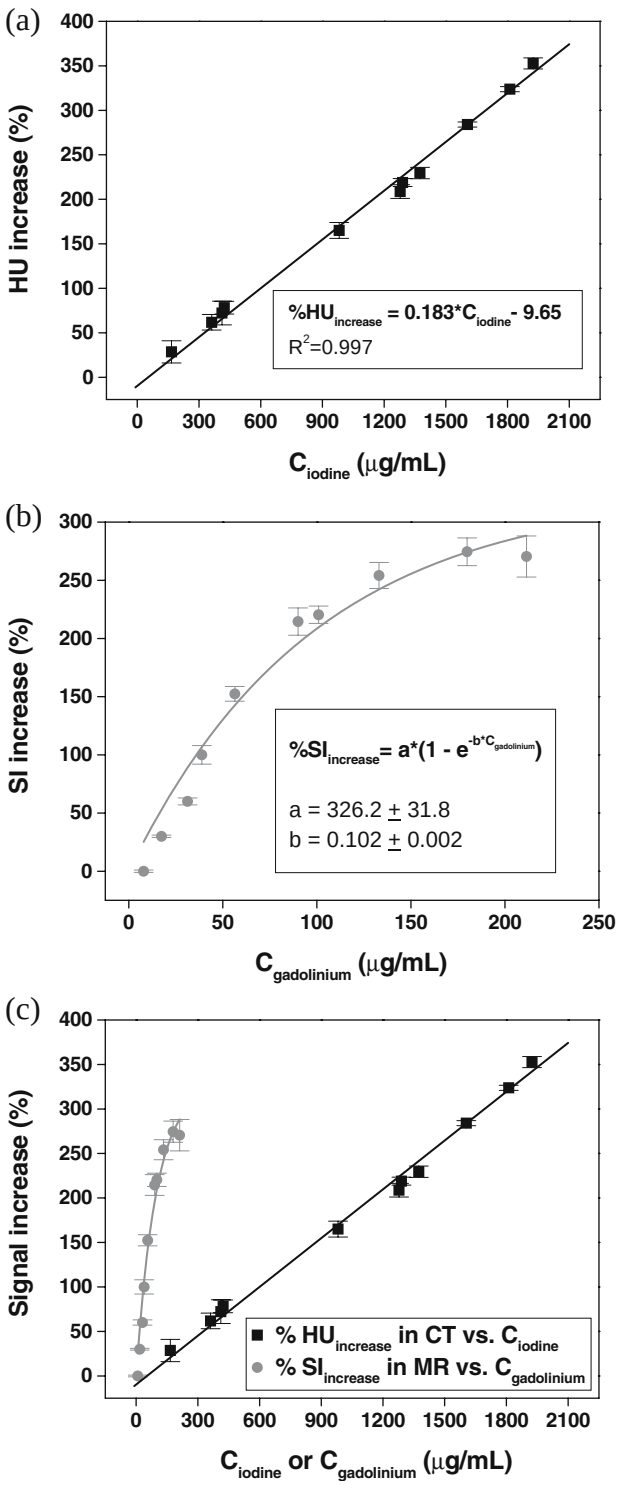

Fig. 4. Plots of the relative change in signal intensity pre- and post-administration of the multimodal liposomal agent **a** in CT versus the measured plasma iodine concentration, **b** in MR versus the measured plasma gadolinium concentration. The $\%HU_{increase}$ in CT was measured using circular regions of interest of 2 mm in diameter in the rabbit aorta and the plasma concentrations of iodine were determined by HPLC (■). The $\%SI_{increase}$ in MR was measured using circular regions of interest of 2 mm in diameter in the rabbit aorta and the plasma concentration of gadolinium was determined by ICP-AES (●). **c** The two plots are combined in a single graph to illustrate the differential response of each modality to different concentrations of the respective contrast agent.

sequentially in CT and MR for a period of 7 days at selected time points both prior to and following administration of the liposome formulation. The clear post-contrast visualization of the rabbit heart, liver and spleen, as well as the transient visualization of the kidneys, is in agreement with the presence of the liposomal iohexol and gadoteridol detected in the same organs in mice (Fig. 2).

At each time point a 1 mL sample of blood was also collected from the rabbit and the plasma concentrations of agents present were quantified using HPLC and ICP-AES analysis. A region of interest of 2 mm in diameter in the rabbit aorta was identified and the signal changes were measured in CT and MR and compared to the concentration values for iodine and gadolinium as determined by analysis of the plasma samples.

The percent signal increases in CT and MR were calculated using Eqs. 3 and 4.

$$\%HU_{increase} = \frac{(HU_t - HU_{t_o})}{HU_{t_o}} \cdot 100 \quad (3)$$

$$\%SI_{increase} = \frac{(SI_t - SI_{t_o})}{SI_{t_o}} \cdot 100 \quad (4)$$

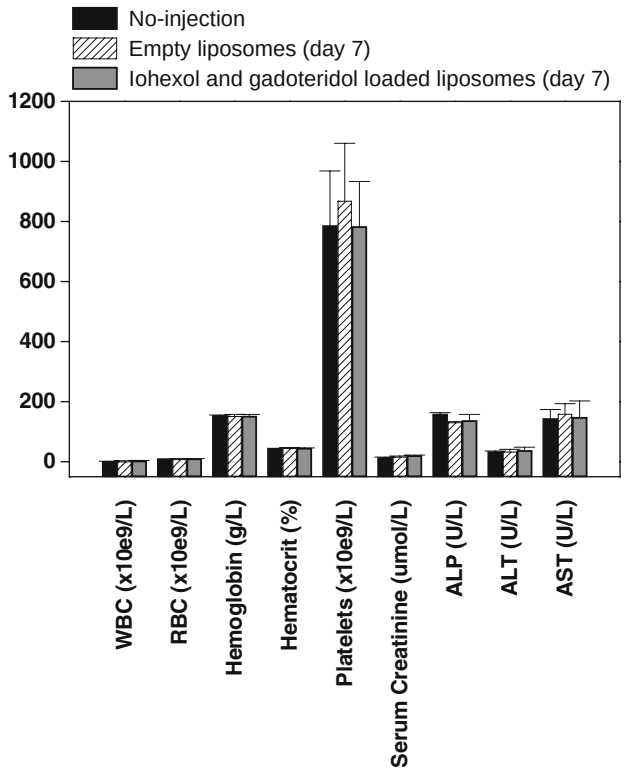

Fig. 5. Summary of the hematological and biochemical evaluation of plasma samples obtained from female Balb-C mice (n=3) 7 days following *1* no treatment, *2* administration of empty liposomes, or *3* administration of liposomes containing both iohexol and gadoteridol. Abbreviations: white blood cell (WBC), red blood cell (RBC), alkaline phosphatase (ALP), alanine transaminase (ALT) and aspartate transaminase (AST). Data are represented as the mean± standard deviation. For all parameters, the differences between the three groups are found to be statistically insignificant using the student t-test (all p-values were greater than 0.05).

Figure 4 includes a plot of the signal changes in CT and MR versus the measured value of the concentration of each respective agent in plasma. A linear correlation (r^2=0.997) was obtained for the $\%HU_{increase}$ measured in CT and the concentration of iodine in the plasma (C_{iodine}). In contrast, an exponential relationship was obtained for the $\%SI_{increase}$ measured in MR and the plasma concentrations of gadolinium ($C_{gadolinium}$). This is a result of the established non-linear relationship between MR signal intensity and gadolinium concentration (43). The successful correlation of the signal changes measured using the imaging systems and the actual concentration of contrast agents detected in the biological samples indicates that this liposome formulation may be suitable for quantitative imaging applications, as well as non-invasive and quantitative CT and MR tracking of these nano-sized vehicles *in vivo*.

Preliminary Evaluation of Acute Toxicity

Figure 5 summarizes the results obtained from the hematological and biochemical analysis of plasma samples obtained one week following administration of both empty liposomes and the liposome formulation of the CT and MR contrast agents. As shown, there were no statistically significant changes (for p=0.05) in the levels of red and white blood cells, hemoglobin, hematocrit, serum creatinine, and various liver enzymes (ALP, ALT and AST), 7 days following administration of the multimodal liposomes in comparison to animals receiving no treatment or those that received the empty liposomes. This analysis provides a preliminary indication of the lack of toxicity and biocompatibility of this formulation.

DISCUSSION

The *in vivo* stability of this liposome formulation was confirmed by evaluation of the PK and biodistribution of the co-encapsulated agents, iohexol and gadoteridol, in healthy mice at various time points following intravenous administration. As shown in Table I, the circulation half-lives for iohexol and gadoteridol were 18.4±2.4 h and 18.1±5.1 h, respectively, when administered in this liposome formulation. When the free agents were administered at the same dose, the distribution (α phase) half-life for the free iohexol was 12.3±0.5 min and 7.6±0.9 min for the free gadoteridol; while, the elimination (β phase) half-lives were 3.0±0.9 h for free iohexol and 3.0±1.3 h for free gadoteridol. Thus, formulation of these agents in the DPPC/CHOL/PEG_{2000}DSPE liposomes significantly increases their circulation half-lives. Though efforts were not put forward to distinguish between the encapsulated and released iohexol or gadoteridol, the similar behavior of iohexol and gadoteridol in terms of accumulation and clearance as detected in the blood, heart and liver strongly suggests that these agents are still co-encapsulated within the internal aqueous volume of the liposomes at the time of measurement. However, iohexol shows an enhanced elimination in both the kidney and the spleen compared to gadoteridol. This may be attributed to the different mechanisms associated with the clearance and metabolism of the individual contrast agents in the kidneys

(44,45) and the spleen. Studies have shown that following intravenous administration approximately 95% of the free agents are cleared though the glomerular filtration process in the kidneys (41,46). Consequently no study has yet been conducted to investigate the clearance and metabolism of iohexol and gadoteridol in the spleen. The alteration in the biodistribution of these agents due to administration in the liposome formulation has now prompted a separate study to investigate the clearance of these agents from the spleen.

The contrast enhancement seen in CT and MR, as shown in Fig. 3, is due to the increased iodine and gadolinium content in the visually enhanced locations. Unlike radionuclide and optical imaging which employ radionuclide tracers and optical labels, CT and MR contrast agents such as iohexol and gadoteridol do not decay or bleach over time. Hence CT and MR are two imaging methods suitable for multi-session longitudinal studies, especially those requiring long imaging sequences. One of the advantages of this dual CT and MR contrast agent system is that the *in vivo* agent concentrations may be monitored over a wider range. Figure 4 shows the ability of MR to estimate *in vivo* gadolinium concentrations ranging from 10 μg/mL to 200 μg/mL, while CT can estimate iodine concentrations from 100 μg/mL to 2000 μg/mL. The lower detection limit presented here corresponds to the iodine or gadolinium concentration needed to generate a signal differential in CT or MR that is greater than the highest noise level. The two imaging modalities may, therefore, detect *in vivo* liposome concentrations that are 1,000 fold lower ($\sim 10^{11}$ liposomes/mL) than the original formulation administered ($\sim 10^{14}$ liposomes/mL). In this way, the dual liposome-based CT and MR contrast agent allows for measurement over a broader concentration range, and also takes advantage of the strengths of each imaging modality. For example, CT provides contrast of the bony structures with high spatial and temporal resolution, while MR allows for better visualization of the soft tissues (9,47,48).

The colloidal size of this multimodal liposomal agent makes it a good intravascular agent (Fig. 3) that may be able to provide reliable estimation of vascular volume. Currently available small molecular weight contrast agents exhibit two-compartment pharmacokinetics, quickly leaking from the blood vessels into the tissue interstitium. Thus, they require complex physiological modeling as well as fast imaging sequences in order to measure their first pass enhancement in studies involving deconvolution of blood vessel permeability and vascular volume in angiogenic tumors (49–51). The successful development of this liposomal agent with prolonged intravascular residence time may be of assistance in obtaining more accurate perfusion and permeability measurements in healthy and diseased tissues, as well as information on physiological processes that occur over a longer time course.

Following characterization of the *in vivo* stability and behavior of this liposome-based system it also became evident that this system may be used as a tool to address unanswered questions that remain surrounding the *in vivo* fate of passively and actively targeted nanocarriers. The clear advantages to the use of imaging methods, over conventional whole organ digestion methods, to map liposome distribution *in vivo* is the non-invasive nature of this approach and the ability to also obtain sub-organ or sub-tissue distribution patterns up to the spatial resolution limit of the imaging system. Specifically in this study, the voxel size achieved was $0.43 \times 0.43 \times 0.625$ mm^3 in CT and $0.86 \times 0.86 \times 1.5$ mm^3 in MR. Potential applications of this CT and MR system include non-invasive assessment of tumor accumulation and distribution of passively and actively targeted liposomes in pre-clinical and clinical settings, development of correlations between tumor penetration of liposomes and the state of tumor vasculature (52). In addition, this multimodal liposome system may be used to assess the performance or behavior of liposomes following administration of different therapies (i.e., anti-angiogenic therapies, radiotherapy and/or chemotherapy), which may ultimately aid in the optimization of the sequence and dosing of combined therapies.

ACKNOWLEDGEMENTS

This work is funded in-part by a CIHR Operating Grant and a CIHR Proof of Principle Grant to D.A. Jaffray and C. Allen, the Premier's Research Excellence Award, the Fidani Chair in Radiation Physics and the Grange Advanced Simulation Initiative. J. Zheng is grateful for the Excellence in Radiation Research for the 21st Century Training Fellowship and the Mitchell Scholarship. The authors would like to thank the UHN animal care staff for their assistance.

REFERENCES

1. W.A. Kalender. X-ray based imaging for computer-assisted surgery. *Minim. Invasive Ther. Allied Technol.* **12**:52–58 (2003).
2. R. B. Sequeiros, R. Ojala, J. Kariniemi, J. Perala, J. Niinimaki, H. Reinikainen, and O. Tervonen. MR-guided interventional procedures: a review. *Acta Radiol.* **46**:576–586 (2005).
3. T. M. Peters. Image-guidance for surgical procedures. *Phys. Med. Biol.* **51**:505–540 (2006).
4. M. A. Rafferty, J. H. Siewerdsen, Y. Chan, M. J. Daly, D. J. Moseley, D. A. Jaffray, and J. C. Irish. Intraoperative cone-beam CT for guidance of temporal bone surgery. *Otolaryngol. Head Neck Surg.* **134**:801–808 (2006).
5. M. Uematsu, M. Sonderegger, A. Shioda, K. Tahara, T. Fukui, Y. Hama, T. Kojima, J. R. Wong, and S. Kusano. Daily positioning accuracy of frameless stereotactic radiation therapy with a fusion of computed tomography and linear accelerator (focal) unit: evaluation of z-axis with a z-marker. *Radiother. Oncol.* **50**:337–339 (1999).
6. D. A. Jaffray, J. H. Siewerdsen, J. W. Wong, and A. A. Martinez. Flat-panel cone-beam computed tomography for image-guided radiation therapy. *Int. J. Radiat. Oncol. Biol. Phys.* **53**:1337–1349 (2002).
7. A. K. Exadaktylos, J. Duwe, F. Eckstein, C. Stoupis, H. Schoenfeld, H. Zimmermann, and T. P. Carrel. The role of contrast-enhanced spiral CT imaging versus chest X-rays in surgical therapeutic concepts and thoracic aortic injury: a 29-year Swiss retrospective analysis of aortic surgery. *Cardiovasc. J. S. Afr.* **16**:162–165 (2005).
8. M. Saeed, D. Saloner, O. Weber, A. Martin, C. Henk, and C. Higgins. MRI in guiding and assessing intramyocardial therapy. *Eur. Radiol.* **15**:851–863 (2005).
9. J. G. Rosenman, E. P. Miller, G. Tracton, and T. J. Cullip. Image registration: an essential part of radiation therapy treatment planning. *Int. J. Radiat. Oncol. Biol. Phys.* **40**:197–205 (1998).
10. P. Leander, P. Hoglund, A. Borseth, Y. Kloster, and A. Berg. A new liposomal liver-specific contrast agent for CT: first human

phase-I clinical trial assessing efficacy and safety. *Eur. Radiol.* **11**:698–704 (2001).
11. C. Y. Kao, E. A. Hoffman, K. C. Beck, R. V. Bellamkonda, and A. V. Annapragada. Long-residence-time nano-scale liposomal iohexol for X-ray-based blood pool imaging. *Acad. Radiol.* **10**:475–483 (2003).
12. S. Erdogan, A. Roby, R. Sawant, J. Hurley, and V. P. Torchilin. Gadolinium-loaded polychelating polymer-containing cancer cell-specific immunoliposomes. *J. Liposome Res.* **16**:45–55 (2006).
13. K. F. Pirollo, J. Dagata, P. Wang, M. Freedman, A. Vladar, S. Fricke, L. Ileva, Q. Zhou, and E. H. Chang. A tumor-targeted nanodelivery system to improve early MRI detection of cancer. *Mol. Imaging* **5**:41–52 (2006).
14. W. J. Mulder, G. J. Strijkers, G. A. Tilborgvan, A. W. Griffioen, and K. Nicolay. Lipid-based nanoparticles for contrast-enhanced MRI and molecular imaging. *NMR Biomed.* **19**:142–164 (2006).
15. S. Mukundan Jr., K. B. Ghaghada, C. T. Badea, C. Y. Kao, L. W. Hedlund, J. M. Provenzale, G. A. Johnson, E. Chen, R. V. Bellamkonda, and A. Annapragada. A liposomal nanoscale contrast agent for preclinical CT in mice. *AJR Am. J. Roentgenol.* **186**:300–307 (2006).
16. M. S. Martina, J. P. Fortin, C. Menager, O. Clement, G. Barratt, C. Grabielle-Madelmont, F. Gazeau, V. Cabuil, and S. Lesieur. Generation of superparamagnetic liposomes revealed as highly efficient MRI contrast agents for *in vivo* imaging. *J. Am. Chem. Soc.* **127**:10676–10685 (2005).
17. C. M. Moran, J. A. Ross, C. Cunningham, M. Butler, T. Anderson, D. Newby, K. A. Fox, and W. N. McDicken. Manufacture and acoustical characterisation of a high-frequency contrast agent for targeting applications. *Ultrasound Med. Biol.* **32**:421–428 (2006).
18. J. Zheng, G. Perkins, A. Kirilova, C. Allen, and D. A. Jaffray. Multimodal contrast agent for combined computed tomography and magnetic resonance imaging applications. *Invest. Radiol.* **41**:339–348 (2006).
19. M. T. Krauze, J. Forsayeth, J. W. Park, and K. S. Bankiewicz. Real-time imaging and quantification of brain delivery of liposomes. *Pharm. Res.* (2006).
20. M. Vaccaro, A. Accardo, D. Tesauro, G. Mangiapia, D. Lof, K. Schillen, O. Soderman, G. Morelli, and L. Paduano. Supramolecular aggregates of amphiphilic gadolinium complexes as blood pool MRI/MRA contrast agents: physicochemical characterization. *Langmuir* **22**:6635–6643 (2006).
21. H. Y. Lee, H. W. Jee, S. M. Seo, B. K. Kwak, G. Khang, and S. H. Cho. Diethylenetriaminepentaacetic acid-gadolinium (DTPA-Gd)-conjugated polysuccinimide derivatives as magnetic resonance imaging contrast agents. *Bioconjug. Chem.* **17**:700–706 (2006).
22. A. Accardo, D. Tesauro, P. Roscigno, E. Gianolio, L. Paduano, G. D'Errico, C. Pedone, and G. Morelli. Physicochemical properties of mixed micellar aggregates containing CCK peptides and Gd complexes designed as tumor specific contrast agents in MRI. *J. Am. Chem. Soc.* **126**:3097–3107 (2004).
23. V. P. Torchilin. PEG-based micelles as carriers of contrast agents for different imaging modalities. *Adv. Drug Deliv. Rev.* **54**:235–252 (2002).
24. V. P. Torchilin, M. D. Frank-Kamenetsky, and G. L. Wolf. CT visualization of blood pool in rats by using long-circulating, iodine-containing micelles. *Acad. Radiol.* **6**:61–65 (1999).
25. D. Zhu, R. D. White, P. A. Hardy, N. Weerapreeyakul, K. Sutthanut, and M. Jay. Biocompatible nanotemplate-engineered nanoparticles containing gadolinium: stability and relaxivity of a potential MRI contrast agent. *J. Nanosci. Nanotechnol.* **6**:996–1003 (2006).
26. I. R. Corbin, H. Li, J. Chen, S. Lund-Katz, R. Zhou, J. D. Glickson, and G. Zheng. Low-density lipoprotein nanoparticles as magnetic resonance imaging contrast agents. *Neoplasia* **8**:488–498 (2006).
27. M. A. McDonald and K. L. Watkin. Investigations into the physicochemical properties of dextran small particulate gadolinium oxide nanoparticles. *Acad. Radiol.* **13**:421–427 (2006).
28. H. Lee, E. Lee, K. Kim do, N. K. Jang, Y. Y. Jeong, and S. Jon. Antibiofouling polymer-coated superparamagnetic iron oxide nanoparticles as potential magnetic resonance contrast agents for *in vivo* cancer imaging. *J. Am. Chem. Soc.* **128**:7383–7389 (2006).
29. J. F. Hainfeld, D. N. Slatkin, T. M. Focella, and H. M. Smilowitz. Gold nanoparticles: a new X-ray contrast agent. *Br. J. Radiol.* **79**:248–253 (2006).
30. O. Rabin, J. Manuel Perez, J. Grimm, G. Wojtkiewicz, and R. Weissleder. An X-ray computed tomography imaging agent based on long-circulating bismuth sulphide nanoparticles. *Nat. Mater.* **5**:118–122 (2006).
31. V. S. Talanov, C. A. Regino, H. Kobayashi, M. Bernardo, P. L. Choyke, and M. W. Brechbiel. Dendrimer-based nanoprobe for dual modality magnetic resonance and fluorescence imaging. *Nano Lett.* **6**:1459–1463 (2006).
32. H. Kobayashi and M. W. Brechbiel. Nano-sized MRI contrast agents with dendrimer cores. *Adv. Drug Deliv. Rev.* **57**:2271–2286 (2005).
33. S. Langereis, Q. G. Lussanetde, M. H. Genderenvan, E. W. Meijer, R. G. Beets-Tan, A. W. Griffioen, J. M. Engelshovenvan, and W. H. Backes. Evaluation of Gd(III)DTPA-terminated poly(propylene imine) dendrimers as contrast agents for MR imaging. *NMR Biomed.* **19**:133–141 (2006).
34. Y. Fu, D. E. Nitecki, D. Maltby, G. H. Simon, K. Berejnoi, H. J. Raatschen, B. M. Yeh, D. M. Shames, and R. C. Brasch. Dendritic iodinated contrast agents with PEG-cores for CT imaging: synthesis and preliminary characterization. *Bioconjug. Chem.* **17**:1043–1056 (2006).
35. M. Port, C. Corot, X. Violas, P. Robert, I. Raynal, and G. Gagneur. How to compare the efficiency of albumin-bound and nonalbumin-bound contrast agents *in vivo*: the concept of dynamic relaxivity. *Invest. Radiol.* **40**:565–573 (2005).
36. Y. Zhang, P. L. Choyke, H. Lu, H. Takahashi, R. B. Mannon, X. Zhang, H. Marcos, K. C. Li, and J. B. Kopp. Detection and localization of proteinuria by dynamic contrast-enhanced magnetic resonance imaging using MS325. *J. Am. Soc. Nephrol.* **16**:1752–1757 (2005).
37. A. M. Morawski, G. A. Lanza, and S. A. Wickline. Targeted contrast agents for magnetic resonance imaging and ultrasound. *Curr. Opin. Biotechnol.* **16**:89–92 (2005).
38. M. A. McDonald and K. L. Watkin. Small particulate gadolinium oxide and gadolinium oxide albumin microspheres as multimodal contrast and therapeutic agents. *Invest. Radiol.* **38**:305–310 (2003).
39. M. F. Kircher, U. Mahmood, R. S. King, R. Weissleder, and L. Josephson. A multimodal nanoparticle for preoperative magnetic resonance imaging and intraoperative optical brain tumor delineation. *Cancer Res.* **63**:8122–8125 (2003).
40. G. R. Norman and D. L. Streiner. *Biostatistics: The Bare Essentials*. B. C. Decker, Hamilton, Canada, 2000.
41. W. Mutzel and U. Speck. Pharmacokinetics and biotransformation of iohexol in the rat and the dog. *Acta Radiol. Suppl.* **362**:87–92 (1980).
42. M. F. Tweedle, X. Zhang, M. Fernandez, P. Wedeking, A. D. Nunn, and H. W. Strauss. A noninvasive method for monitoring renal status at bedside. *Invest. Radiol.* **32**:802–805 (1997).
43. M. Heilmann, F. Kiessling, M. Enderlin, and L. R. Schad. Determination of pharmacokinetic parameters in DCE MRI: consequence of nonlinearity between contrast agent concentration and signal intensity. *Invest. Radiol.* **41**:536–543 (2006).
44. S. J. McLachlan, S. Eaton, and D. N. SimoneDe. Pharmacokinetic behavior of gadoteridol injection. *Invest. Radiol.* **27** (Suppl 1): S12–S15 (1992).
45. A. Arvidsson and A. Hedman. Plasma and renal clearance of iohexol—a study on the reproducibility of a method for the glomerular filtration rate. *Scand. J. Clin. Lab. Invest.* **50**:757–761 (1990).
46. M. F. Tweedle. The ProHance story: the making of a novel MRI contrast agent. *Eur. Radiol.* **7** (Suppl 5): 225–230 (1997).
47. C. Rasch, I. Barillot, P. Remeijer, A. Touw, M. Herkvan, and J. V. Lebesque. Definition of the prostate in CT and MRI: a multi-observer study. *Int. J. Radiat. Oncol. Biol. Phys.* **43**:57–66 (1999).

48. H. U. Kauczor. Multimodal imaging and computer assisted diagnosis for functional tumour characterisation. *Cancer Imaging* **5**:46–50 (2005).
49. P. L. Choyke. Contrast agents for imaging tumor angiogenesis: is bigger better?. *Radiology* **235**:1–2 (2005).
50. M. R. Dreher, W. Liu, C. R. Michelich, M. W. Dewhirst, F. Yuan, and A. Chilkoti. Tumor vascular permeability, accumulation, and penetration of macromolecular drug carriers. *J. Natl. Cancer Inst.* **98**:335–344 (2006).
51. K. A. Miles. Functional computed tomography in oncology. *Eur. J. Cancer* **38**:2079–2084 (2002).
52. H. E. Daldrup-Link, G. H. Simon, and R. C. Brasch. Imaging of tumor angiogenesis: current approaches and future prospects. *Curr. Pharm. Des.* **12**:2661–2672 (2006).